Optimizing Repair Welding Techniques in Cast Steels—Part I

Maximum hardness in the HAZ can be predicted to within a few Rc points with the help of a technique developed to measure temperatures in the HAZ at the fusion boundary

BY D. K. AIDUN AND W. F. SAVAGE

ABSTRACT. A simple and inexpensive technique was developed using thermocouples to measure the maximum average temperature in the HAZ next to the fusion boundary during the simulated repair welding of steel castings. The measurement was taken by inserting the wires through adjacent holes until their ends protruded through the top surface of the specimen.

A logarithmic equation was obtained to describe the relationship between the instantaneous temperature (T_i) and the time (t) after arc cutoff. This relationship describes the approximate thermal cycle during cooling between 1000 and 700°F (538 and 371°C), the critical transformation temperature range for most steels. This approximation is accurate enough to estimate the predicted maximum hardness in the homogeneous coarse-grained heat-affected zone to within a few R_c points.

A relationship was then developed (for stationary and linear welds) to estimate the cooling rate next to the fusion boundary using three simultaneous variables: section thickness (TH), initial plate temperature (T_o), and weld energy input (EIS, TEIL).

Introduction

Despite forty years of research on the subject of hydrogen-induced cracking (HIC), it continues to be a major problem in the welding of steel. In general, the susceptibility to HIC increases with increase in the hardness of the microstructure in the weld heat-affected zone (HAZ); thus, to prevent HIC in steels one should reduce the maximum hardness level in the HAZ or reduce constraint, use a low H_2 electrode, etc. The critical level of diffusible hydrogen in a weldment is influenced by the toughness and ductility of the microstructure of the heat-affected zone (HAZ). Increasing the maximum hardness level in the HAZ lowers the critical hydrogen concentration required to cause HIC.

It is a basic principle of metallurgy that, in a steel of a given hardenability, grain size and carbon content, equivalent cooling conditions will always produce equivalent microstructures and, therefore, the same hardness. This principle provides the basis for the Jominy Hardenability Test (Ref. 1) which provides, in a single test specimen, reproducible cooling rates ranging from those achieved with the most vigorous of water quenches to those associated with cooling in still air.

Because the cooling rates (CR) at various distances from the water-quenched end (JD) are known, the cooling rate required to produce a particular hardness in a steel of any given hardenability can be deduced from a knowledge of the value of Jominy distance (JD) at which that hardness is found. If, in addition, there are data relating the maximum cooling rates experienced in the HAZ to weld geometry and welding conditions, welding procedures can be selected to ensure that the maximum HAZ hardness will not exceed a particular hardness level.

Unfortunately, it is rarely possible to obtain Jominy hardenability test data for the particular steel to be welded. However, Field (Ref. 2) has published a procedure for calculating Jominy hardenability data from chemical composition and ASTM grain size. And although such hardenability data are for long time austenization during heat treatment, they can be applied to HAZ's, provided partial homogenization takes place. In the case of this study the ASTM grain size was 5.

In 1943, Hess *et al.* (Ref. 3) published the results of an extensive study of the effects of weld energy input, plate thickness, initial plate temperature, and electrode size on the maximum cooling rates experienced in the HAZ of welded butt joints in steel plates. The paper contained a series of tables summarizing the effect of these variables on the maximum cooling rate in the HAZ. In a subsequent article, Hess *et al.* (Ref. 4) summarized similar information for fillet welds in steel plates. These data, when coupled with the Jominy hardenability behavior of a given steel, can be used to predict the maximum hardness which will be produced in the HAZ by a particular set of welding variables.

Since 1943 several investigators (Refs. 5-8) have tried to develop a simpler method of predicting the HAZ microstructure in the weldments with varying degrees of success. However, to date no comprehensive treatment of the effect of welding procedures on the HAZ microstructure of repair welds in steel castings has been attempted.

This paper and a subsequent paper (Part II) deal with a solution to the problems involved in optimizing repair welding procedures for steel castings and steels.

Objectives

The objectives of this portion of the investigation were:

1. To develop a reliable and reproducible technique for measuring cooling rates in the HAZ of simulated repair welds

D. K. AIDUN is Assistant Professor, Mechanical and Industrial Engineering Department, Clarkson University, Potsdam, New York; and W. F. SAVAGE is Professor Emeritus, Rensselaer Polytechnic Institute, Troy, New York.

Table 1—Chemical Composition (Wt-%), Initial Hardness (IH), and Ideal Critical Diameter (D_I) by Heat Numbers

	9861	32	27	1	0
C	0.24	0.32	0.31	0.21	0.26
Mn	0.77	1.15	1.57	1.24	0.74
P	0.038	0.017	0.013	0.018	0.021
S	0.029	0.017	0.013	0.031	0.028
Si	0.49	0.54	0.50	0.51	0.40
Ni	0.16	–	0.03	0.07	0.04
Cr	0.32	0.13	0.14	0.20	0.31
Mo	0.08	0.22	0.10	0.03	0.02
Cu	0.08	0.04	0.04	0.04	0.03
Al	0.056	0.078	0.054	0.11	0.075
IH (Rc)	47	51	51	45	48
D_I (inc.)	2.06	3.17	3.51	2.05	1.61

for various defect geometries (circular and linear) and welding conditions.

2. To develop a simple mathematical relationship for predicting the cooling rates in the important transformation range for the HAZ of simulated repair welds in terms of weld geometry and welding conditions.

3. To develop a system for selecting welding conditions which assure a maximum hardness in the HAZ of repair welds below an appropriate critical hardness.

Materials and Specimen Preparation

Five heats of cast steel were used in this investigation. Table 1 lists the chemical composition, initial hardness, IH, (*i.e.*, the hardness of martensite) and ideal critical diameter, D_I (based upon 50% martensite), for all five heats.

Heat 9861 was received in the form of keel blocks from which specimens 2¼ × 2¼ × 1 in. (57.2 × 57.2 × 25.4 mm) were machined. The other four heats were supplied in the form of cast coupons approximately 10¼ × 4¼ × ¾ in. (260 × 108 × 19 mm). A pair of 0.049 in. (1.25 mm) diameter holes were then drilled completely through each test specimen at selected sites within the simulated repair weld geometry for cooling rate measurements.

Temperature Measurement

Temperature measurements were made for each of the simulated repair weld geometries as follows:

1. Asbestos-and-glass-insulated 0.032 in. (0.83 mm) diameter wires of chromel-alumel were threaded through adjacent holes until their ends protruded through the top surface of the specimen; wires were constrained in this position by bending.

2. The repair weld was then made and the weld deposit provided the hot-junction between the chromel-alumel wires. Figure 1 shows the details of typical thermocouple locations used in this investigation for a simple bead-on-plate geometry (Fig. 1A) and for a more complicated weld geometry, such as a cavity—Fig. 1B. The thermocouple outputs were recorded as a function of time with a direct-developing, multichannel oscillograph.

The various welding conditions used during temperature measurements in stationary welds (SW) and linear welds (LW) are summarized in Table 2.

Results and Discussions

Cooling Rate Measurements

One of the initial objectives of this investigation was to develop a reliable and reproducible method of measuring temperature in the HAZ. Other investigators (Refs. 3, 5) had percussion welded small-diameter thermocouples (0.010 in., *i.e.*, 0.25 mm) to the bottom of holes drilled to within 1/32 in. (0.79 mm) from the surface of the plate. Because of steep temperature gradients, the temperature measurements were extremely dependent on the location of the hot-junction relative to the fusion boundary. The difficulty in determining the exact location of the hot-junction resulted in unacceptably large experimental errors in the temperature measurements.

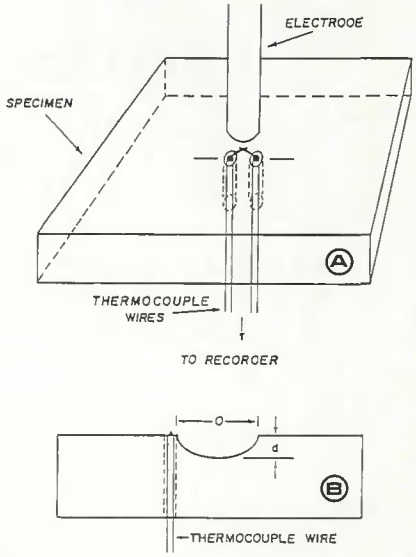

Fig. 1—Schematic diagram of thermocouple locations with respect to electrode for temperature measurements

The technique used in this investigation provided a consistent time-temperature profile which in turn produced reliable cooling-rate data for the HAZ. The result of a typical set of measurements are shown in Table 3. The experiments were performed using identical welding conditions and the same specimen geometry.

From a large number of temperature measurements made on simulated repair welds, it was found that a logarithmic relationship can be employed to approximate the thermal cycle experienced upon cooling from 1000 to 700°F (538 to 371°C). This range of temperature corresponds to the important elevated transformation temperature range for most steel castings. The time-temperature relationships developed for both the stationary welds (SW) and for linear welds (LW) are as follows:

1. For stationary welds: $T_i - T_o = A + B \ln t$, $700 \leq T \leq 1000°F$; (1)

2. For linear welds: $T_i = A' + B \ln t$, $700 \leq T \leq 1000°F$; (2)

where T_i = instantaneous temperature (°F) at time, t; T_o = initial plate temperature (°F); t = time after arc cut off (seconds, s); and A, A′ and B are coefficients (°F).

Equations (1) and (2) are valid for t > 1 second(s) within the above temperature range. The logarithmic relationship was adopted, since it is a simple equation to use, gives a good approximation of the

Table 2—Range of Welding Conditions Used in the Temperature Measurement Studies

	Stationary weld	Linear weld
Arc current, A	125,220	165,220
Arc voltage, V	22,24	22,25
Arc time t_a, s	5 to 80	–
Travel speed TS, ipm	–	2.5 to 10
Weld length dw, in.	–	2.0 to 8.0
Initial plate temperature T_o, °F	78 to 400	78 to 550
Thickness TH, in.	½ to 1⅛	¾ to 1⅛

observed thermal cycle during cooling within the transformation temperature range (Fig. 2), and has the distinct advantage of providing a simple expression for the cooling rate, $\frac{dT}{dt}$, at any instantaneous temperature, T_i. Note that differentiation of both equations (1) and (2) gives:

$$\frac{dT}{dt}\Big|_{T_i} = \frac{B}{t} \qquad (3)$$

Rosenthal (Ref. 9) and others have done extensive heat-transfer studies on arc welding, assuming various boundary conditions and types of heat source. However, as the boundary conditions change, the heat-transfer equations must be modified to meet the required boundary values, and, the differential equations become rather complex. Therefore, although the simple logarithmic equations are empirical, they were found to be in agreement with the measured data within the range of temperature of interest. Note that, although significant deviations from the actual temperature are predicted by the logarithmic equation both above 1000°F (538°C) and below 700°F (371°C), the predicted and measured time-temperature data were found to agree closely within these limits.

Figure 3 consists of plots of T_i-T_o as calculated from the logarithmic equation for three different combinations of arc time, t_a, and initial plate temperature, T_o (solid lines). The open circles represent actual temperature measurements. The amount of scatter in the experimental data is represented by the size of the circles in these plots. Although only the weld time changes in comparing welding conditions in Figs. 3A and 3B, the values for coefficients A and B are vastly different. This emphasizes the dependence of coefficients A and B on the weld energy input at constant plate thickness and initial plate temperature (T_o). Comparison of plots in Figs. 3B and 3C reveals the influence of initial plate temperature on A and B at constant plate thickness and weld energy input. Additional experiments were performed to determine the influence of plate thickness and the geometry of the simulated defects.

From these experiments it was found that the weld energy input is the dominant variable influencing the maximum cooling rate in the weld heat-affected zone. For stationary welds, the energy input, EIS, in joules, is defined as follows:

$$EIS = I \times V \times t_a, \qquad (4)$$

where: I = arc current in amperes (A); V = arc voltage in volts (V); t_a = arc time, s.

For linear welds, the energy input per linear inch of weld, EIL, in joules/inch (J/in.), is defined as follows:

$$EIL = \frac{I \times V}{TS} \times 60 \qquad (5a)$$

where: I = arc current, A; V = arc voltage, V; TS = travel speed, ipm.

Total linear weld energy input, TEIL in joules, can be written as

TEIL = (EIL) dw

where: dw = weld length, in. (5b)

Figure 4 summarizes the effects of weld energy input and initial plate temperature, respectively, on the cooling rate for stationary repair welds made in 1.0 in. (25.4 mm) thick plate. Attention is drawn to the extremely rapid increase in the cooling rate as the weld energy input is reduced below 30 kJ. This emphasizes the danger of making small "cosmetic" repairs which involve short arc times and, therefore, low weld energy inputs.

Table 4 summarizes the influence of section thickness, arc time, and initial plate temperature on the cooling rates measured at the fusion boundary of stationary repair welds. Note that, at instantaneous temperatures between 700 and 1000°F (371 and 538°C), arc times of 8 s in 1.0 in. (25.4 mm) plate and 5 s in 0.5 in. (12.7 mm) plate gave almost identical cooling rates when T_o was 78°F (25.6°C). Note also that in 1.0 in. thick plate, arc times of 40 s with T_o = 78°F (25.6°C) and 30 s with T_o = 200°F (93°C) gave similar cooling rates. It is also of interest that in 1.0 in. (25.4 mm) thick plate, arc times of 80 s with T_o = 78°F (25.6°C) and 30 s with T_o = 400°F (204°C) gave almost identical cooling-rate values.

From the above representative data, it is clear that for a given section thickness the cooling rates can be controlled by appropriate manipulation of the welding variables. Since the cooling rate through the transformation temperature range determines the microstructure and mechanical properties of the HAZ, it follows that both can be controlled by the proper choice of welding procedures.

Table 5 lists the variables that influence the cooling rates in the HAZ of repair welds.

The coefficients A, A′ and B in equations (1) and (2) are dependent on the specific welding conditions (W_c) which include weld energy input (EIS or TEIL), section thickness (TH), and initial plate temperature (T_o). Various mathematical equations have been developed to

Table 3—Typical Results of Cooling Rate Measurements From Two Identical Simulated Repair Welds

Welding conditions (stationary weld):

Arc current, A	125
Arc voltage, V	22
Arc time t_a, s	30
Initial plate temperature T_o, °F	78
Section thickness TH, in.	1.0

Measured cooling rates at various temperatures, °F/s[a]:

Experiment	700°F	800°F	900°F	1000°F
1	27	32	38	44
2	28	33	39	46

[a]The cooling rates were calculated from the time-temperature profile of the HAZ.

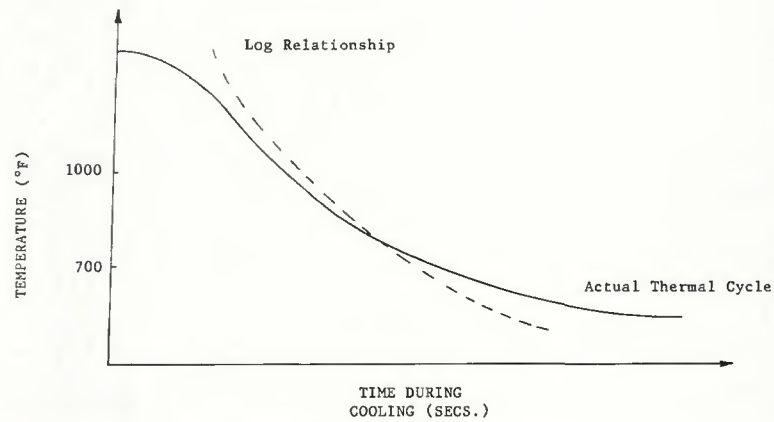

Fig. 2—Schematic correlation between the log relationships and actual thermal cycle in the HAZ

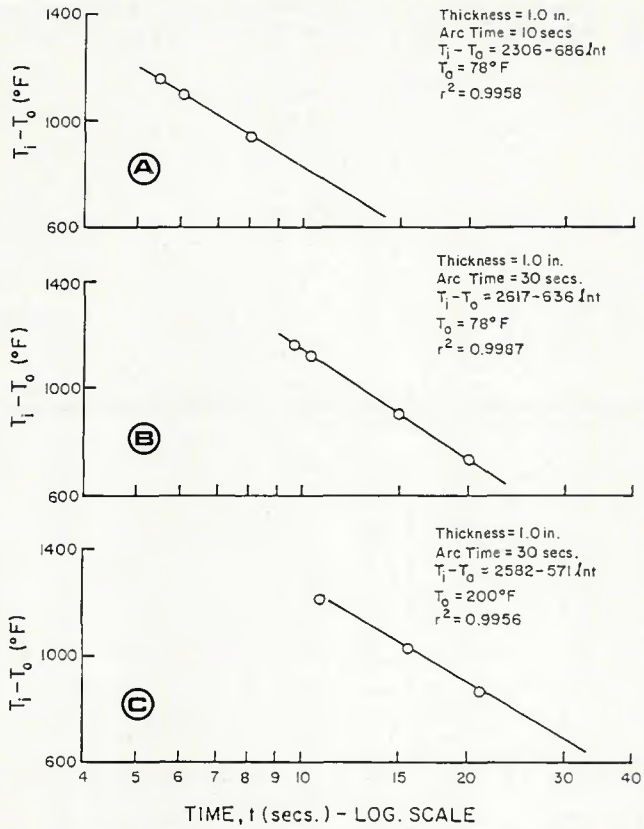

Fig. 3 — Typical plots of $T_i - T_o$ vs. log t for stationary welds using 125A at 22 V

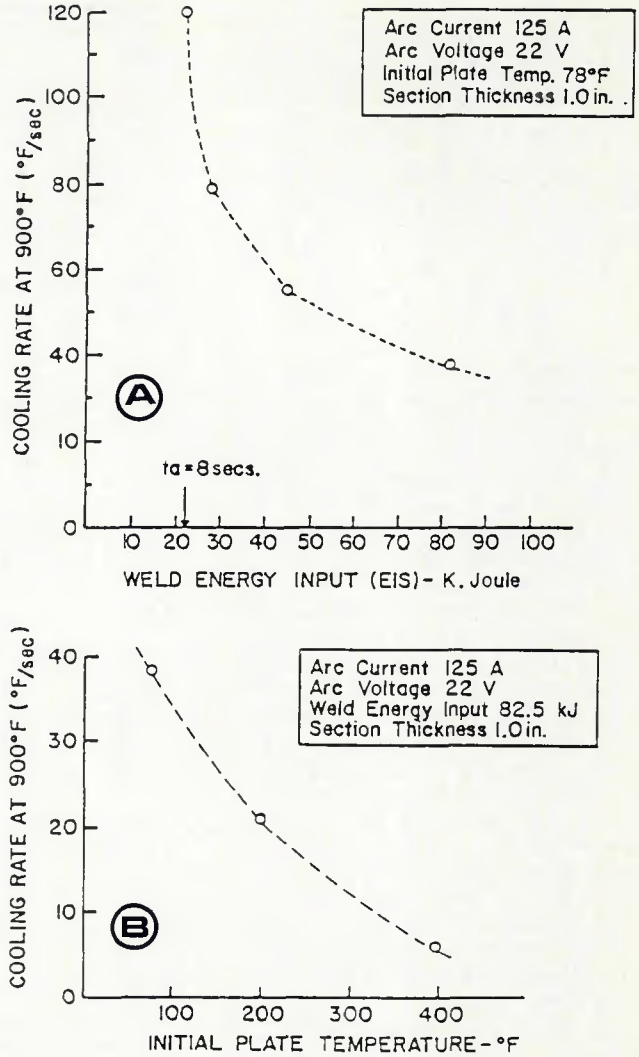

Fig. 4 (right) — Effect of energy input and initial plate temperature on cooling rates in stationary repair welds

Table 4—Summary of the Effect of Section Thickness, Arc Time, and Preheat Temperature T_o on Cooling Rates at Various Temperatures

Fixed conditions for stationary weld:

Arc current, A 125
Arc voltage, V 22

Measured cooling rates at various temperatures, °F/s[a]:

Preheat T_o, °F	Thickness TH, in.	Arc time T_a, s	700°F	800°F	900°F	1000°F
78	0.5	5	85	101	121	145
78	0.5	8	49	58	70	84
78	1.0	8	87	102	120	140
78	1.0	10	59	69	79	91
78	1.0	20	30	36	44	54
78	1.0	30	27	32	38	44
78	1.0	40	13	16	20	24
78	1.0	80	4	4	6	7
200	1.0	30	15	18	21	25
400	1.0	30	4	5	6	7

[a]The cooling rates were measured from the time-temperature profile of the HAZ. Time constant for 1/32 in. (0.79 mm) diameter welding wire of approx. 1.9 s was ignored in the calculations.

express the relationship between the coefficients and the welding conditions. The form of power expressions given in equation (6) describes the relationship between the coefficients and the welding variables with a correlation coefficient, $r^2 > 0.99$, so that:

$$A, A' \text{ or } |B| = a(W_c)^b \quad (6)$$

Tables 6 through 9 show typical examples of the relationships derived for coefficients A, A′ and |B| in terms of the four factors influencing the cooling rate, the comparisons of cooling data calculated, using these relationships, and the actual measured values.

Specifically, Table 6 is a typical example of the calculation of the effect of arc time t_a. Table 7 then shows the effect of weld length, dw, on the coefficients A′ and |B| for a typical set of linear welds in a ¾ in. (19.1 mm) thick plate with calculated and measured values of the cooling rate included. Table 8 shows the effect of section thickness, TH, and Table 9 shows

Table 5—Factors Influencing the Maximum Cooling Rate In the Weld Heat-Affected Zone[a]

1. Weld energy input, EIS or TEIL
2. Section thickness, TH
3. Initial plate temperature, T_o
4. Joint geometry

[a]For carbon and low-alloy steels the thermal and electrical characteristics are virtually independent of composition and, therefore, the cooling rates and I^2R heating behavior are not dependent on the chemical composition.

the effect of initial plate temperature, T_o, on the coefficients A and |B| for a typical set of stationary welds in a 1.0 in. (25.4 mm) thick plate; calculated and measured values of cooling rate are included in each table.

In this fashion, it is possible to generate empirical relationships for the coefficients A, A′ and B in terms of welding conditions and joint geometry. By solving these relationships for a particular set of welding parameters and substituting the results in equations (1) or (2), the time, t, after arc cut-off required for the temperature to reach a given instantaneous value, T_i, can be calculated. By substituting the values of B and t in equation (3), the cooling rate, $\left.\frac{dT}{dt}\right|_{Ti}$ at that instantaneous temperature, T_i, can then be calculated.

Hardenability Calculations

Hardenability is defined as an index of the ease of formation of martensite in a steel. In general, hardenability is increased by:

1. Increasing the amount of carbon dissolved in the austenite.
2. Increasing the amount of alloying elements dissolved in the austenite (except for cobalt).
3. Increasing the austenite grain size.
4. Increasing the homogeneity of the austenite.

One commonly used index of hardenability is the ideal critical diameter, D_I. This is defined as the diameter of bar that will just achieve a given critical hardness at its center when quenched in a hypothetical ideal quenching medium that lowers the surface temperature of the bar to that of the bath instantaneously.

While numerous empirical relationships have been developed for calculating D_I from the chemical analyses and grain size of a steel, the method published by Fields (Ref. 2) has been adopted in this work.* Although the homogeneity of austenite formed in weld HAZ is uncertain, experience suggests that a reasonable engineering estimate of D_I (based

*See ASTM A255.

Table 6—The Effects of Arc Time, t_a, (or EIS) on the Coefficients A and |B| for Stationary Welds

Welding conditions:

E7018 electrode diameter, in.	3/16
Arc current, A	220
Arc voltage, V	25
Initial plate temperature T_o, °F	78
Specimen size, in.	5.0 × 4.0 × 0.75

$A = 2023\ (t_a)^{0.105}$ (7)

$|B| = 987\ (t_a)^{-0.106}$ (8)

(Valid range: $5 \leq t_a \leq 40$ s.)

Typical cooling rates at 800 and 900°F, °F/s:

	800°F		900°F	
	Measured	Calculated	Measured	Calculated
t_a, s				
5	84	83	94	95
10	49	50	57	58
40	15	15	17	17

Table 7—The Effect of Weld Length, dw, on the Coefficients A′ and |B| for Linear Welds

Welding conditions:

E7018 electrode diameter, in.	3/16
Arc current, A	220
Arc voltage, V	25
Travel speed TS, ipm	5
Initial plate temperature T_o, °F	78
Specimen size, in.	10.0 × 4.0 × 0.75 in.

$A' = 4402\ (dw)^{-0.230}$ (9)

$|B| = 1246\ (dw)^{-0.453}$ (10)

(Valid range $2.0 \leq dw \leq 6.0$ in.)

Typical cooling rates at 800 and 900°F, °F/s:

	800°F		900°F	
	Measured	Calculated	Measured	Calculated
dw, in.				
3.0	18	24	21	27
6.0	14	12	16	15

Table 8—The Effect of Section Thickness, TH, on the Coefficients A and |B| for Stationary Welds

Welding conditions:

E7018 electrode diameter, in.	3/16
Arc current, A	220
Arc voltage, V	25
Arc time t_a, s	10
Initial Plate Temperature T_o, °F	78
Specimen size, in.	5.0 × 4.0 × TH

$A = 2427\ (TH)^{-0.112}$ (11)

$|B| = 690\ (TH)^{0.075}$ (12)

(Valid range $0.25 \leq TH \leq 1.00$ in.)

Typical cooling rates at 800 and 900°F, °F/s:

	800°F		900°F	
	Measured	Calculated	Measured	Calculated
TH, in.				
0.25	21	21	24	25
0.50	35	36	39	41
0.75	49	48	57	56

Table 9—The Effect of Initial Plate Temperature, T_o on the Coefficients A and |B| for Stationary Welds

Welding conditions:

E6010 electrode diameter, in.	5/32
Arc current, A	125
Arc voltage, V	22
Arc time t_a, s	30
Specimen size, in.	2.25 × 2.25 × 1.00 (TH)

$A = 3462\ (T_o)^{-0.060}$ (13)

$|B| = 2023\ (T_o)^{-0.256}$ (14)

(Valid range $78 \leq T_o \leq 400°F$) (15)

Typical cooling rates at 800 and 900°F, °F/s:

	800°F		900°F	
	Measured	Calculated	Measured	Calculated
T_o, °F				
78	32	35	38	41
200	18	13	21	16
400	5	4	6	5

Table 10—Summary of Equations for Calculating Ideal Critical Diameter From Chemical Composition and Grain Size

D_I (in.) $= \pi_i M_i = M_{C,n} \times M_{Mn} \times \ldots$ (15)

$M_{C,n} = [0.397\ (\%C)^{0.504}]\ (1.08)^{(5-n)}$ (16)[a]

$Mn \leq 1.20\%\ M_{Mn} = 1.0 + 3.333\ (\%Mn)$ (17a)

$Mn > 1.20\%\ M_{Mn} = 5.10\ (\%Mn) - 1.12$ (17b)

$M_{Si} = 1.0 + 0.700\ (\%Si)$ (18)

$M_{Ni} = 1.0 + 0.364\ (\%Ni)$ (19)

$M_{Cr} = 1.0 + 2.160\ (\%Cr)$ (20)

$M_{Mo} = 1.0 + 3.000\ (\%Mo)$ (21)

where Mi is the multiplying factor for element i; i is C, Mn, Si, Ni, Cr, Mo; n is ASTM G.S. no.; π_i is the product of the multiplying factors.

[a]Experience has shown that underestimating the grain size as ASTM #5 compensates for the lack of homogeneity in the austenite produced in the coarse-grained region of the HAZ.

upon a hardness criterion corresponding to that of a microstructure consisting of 50% martensite and 50% other transformation products) can be obtained using the method summarized in Table 10.

Equations (15) to (21) for the multiplying factors were derived by curve fitting the data published by Fields. Equation (16), for calculating the value of $M_{C,n}$ is based upon an assumed ASTM grain size number of 5 (see Table 10 footnote). Fields also developed a method for calculating the Jominy hardenability curve from the calculated value of D_I. In this method, the hardness expected at a given location on a Jominy bar is defined as a distance hardness, DH. A table was then prepared for various values of D_I and Jominy distance wherein:

IH = the initial hardness = the hardness expected at 1/16 in. on the Jominy bar, presumably that of 100% martensite.

Savage (Ref. 10), in an unpublished work, has cross-plotted and curve-fitted these data as well as the published values of IH for various carbon contents. The resulting equations are summarized in Table 11. Equation 22 permits the calculation of IH for any carbon content between 0.01 and 0.80%. With the aid of equation (23), it is possible to calculate the Jominy distance, JD, at which a given distance hardness, DH, can be found for a steel with a calculated hardenability of D_I. Equation (24) permits the calculation of IH/DH for a given JD and D_I.

To complete the system for predicting the hardness of the weld HAZ, it is only necessary to correlate the cooling rates at various locations on the Jominy bar with those associated with the HAZ. This link is provided by the following relationship between the cooling rate, CR, at 900°F (482°C), and the Jominy distance, JD, in sixteenths of an inch:

$$CR = 6.353\ \left(\frac{16}{JD}\right)^{1.32} \qquad (25)$$

This may be rearranged so that:

$$JD = \exp\left[\frac{5.50 - \ln(CR)}{1.32}\right]. \qquad (26)$$

Table 11—Summary of Equations Developed for Calculating Jominy Data From Ideal Critical Diameter and the Carbon Content

$$IH\ (Rc) = \frac{1}{0.0126 - 0.0061\ \ln(\%C)} \qquad (22)$$

$$JD = \frac{\left(\frac{IH}{DH}\right) - c}{d}\ \text{JD in 16th inches} \qquad (23)^{[a]}$$

where $c = 0.324 + 0.227\ (D_I)$ for $D_I \leq 2.30$ in.

$c = 0.850$ for $D_I > 2.30$ in.

$d = 0.405\ (D_I)^{-1.614}$ for all D_I values

[a]Equation (23) may be rearranged to give:

$$\frac{IH}{DH} = c + d(JD) \qquad (24)$$

System for Prediction of Maximum Hardness in the Weld Heat-Affected Zone

In order to predict the maximum hardness in the HAZ of a particular weld, the following system can be used:

1. Calculate the maximum cooling rate in the weld HAZ using the weld energy input (EIS or TEIL), section thickness (TH), and initial plate temperature (T_o) values for equations (1) (or 2) and (3).
2. Calculate the Jominy distance at which this cooling rate is found with the aid of equation (26).
3. Calculate D_I for the steel using the equations (15) to (21) in Table 10.
4. Calculate IH/DH with the aid of equation (24) in Table 11.
5. Calculate IH from the carbon content using equation (22) in Table 11.
6. Divide the IH value from step 5 by the $\frac{IH}{DH}$ ratio from step 4 to obtain DH. This value will be the estimated maximum hardness in the coarse-grained region of the HAZ adjacent to the fusion boundary.

To test the above system, eight specimens of various thicknesses from heat 9861 were welded with different weld energy inputs and initial plate temperatures (preheat temperatures). The maximum VHN (1 kg, *i.e.*, 2.2 lb) hardnesses in the HAZ were then measured, converted to the equivalent Rc values, and compared to the maximum hardness levels in

Table 12—Comparison of Measured and Predicted Maximum Hardness Levels in the HAZ of Stationary Test Welds[a]

Thickness TH, in.	Arc time t_a, s	Preheat temperature T_o, °F	Maximum HAZ hardness: Measured VHN, 1 kg	Measured Rc	Predicted Rc
0.5	5	78	(493)	48	46
0.5	8	78	(429)	43	43
1.0	8	78	(490)	48	46
1.0	10	78	(446)	43	44
1.0	20	78	(405)	41	40
1.0	30	78	(390)	39	38
1.0	30	200	(302)	30	32
1.0	30	400	(233)	18	19

[a]Welding conditions: arc current – 125 A; arc voltage – 22 V.

the HAZ (predicted by the system described above). Table 12 compares the measured and predicted hardness values. Note that, among the eight test welds, the maximum deviation between predicted and measured values was ± 2 Rc points. This by no means represents the maximum possible deviation.

Figure 5 shows the weld HAZ microstructures adjacent to the fusion boundary in 1.0 in. (25.4 mm) thick plate specimens welded with 125 A, 22 V, and various combinations of arc time (t_a) and initial plate temperature (T_o). Figure 5A (t_a = 10 s, T_o = 78°F, *i.e.*, 25.6°C) shows a fully martensite structure which exhibited a hardness of 43 Rc (predicted hardness, 44 Rc). Figure 5B which was subjected to higher weld energy input (t_a = 30 s, T_o = 78°F/25.6°C), shows a mixture of Widmanstätten ferrite (white needles), bainite and martensite with a measured hardness of 39 Rc (predicted hardness, 38 Rc). Figure 5C (t_a = 30 s, T_o = 200°F, *i.e.*, 93°C) shows a mixture of Widmanstätten ferrite and fine pearlite with a measured hardness of 30 Rc (predicted hardness, 32 Rc). The drop in the hardness between 5b and 5c is a result of the increase in the initial plate temperature which decreases the cooling rate in the transformation temperature range from 38 to 21°F/s (21 to 11.7°C/s) at 900°F, *i.e.*, 482°C (refer to Table 4).

Development of Generalized Relationships for Predicting Cooling Rates In Repair Welds

Because equation (6) is only valid for one variable, an empirical relationship of a series type was developed by treating the various values of A, A′ and |B| for the different welding conditions studied and summarized in Table 13; the valid ranges

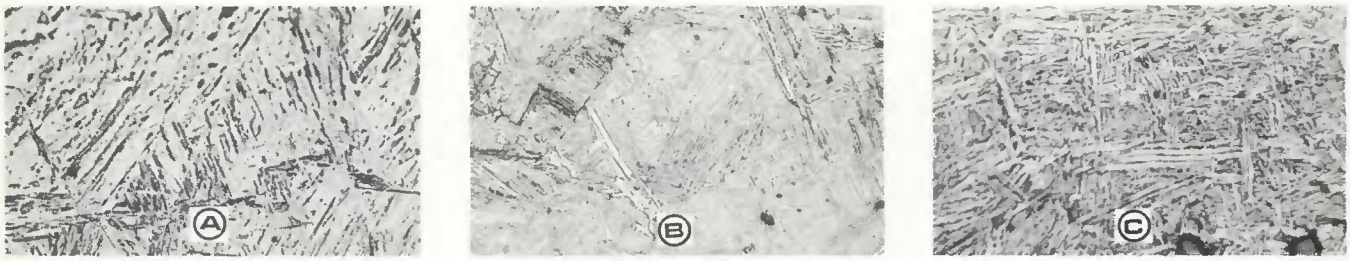

Fig. 5 — HAZ microstructure produced adjacent to the fusion zone by stationary welds in 1.0 in. (25.4 mm) thick heat 9861 using 125 A, 22 V, and the indicated values of arc time, t_a, and initial plate temperature, T_o: A – t_a = 10 s, T_o = 78°F; B – t_a = 30 s, T_o = 78°F; C – t_a = 30 s, T_o = 200°F. 2% nital, ×500 (reduced 37% on reproduction)

Table 13—Summary of General Form and Limitations for the Series-Type Equations for Calculating The Coefficients Used in Obtaining Weld Cooling Rates

$$(A_i, A_i' \text{ or } |B_i|)/_T' = A_1\left(\frac{TH_i}{TH'}\right)^2 + A_2\left(\frac{TH_i}{TH'}\right) + A_3\left(\frac{T'}{T_i}\right)^2 + A_4\left(\frac{T'}{T_i}\right) + A_5\left(\frac{IE'}{IE_i}\right)^2 + A_6\left(\frac{IE'}{IE_i}\right) + A_7\left(\frac{TH_i}{Th'}\right)\left(\frac{T'}{T_i}\right) + A_8\left(\frac{TH_i}{TH'}\right)\left(\frac{IE'}{IE_i}\right) + A_9\left(\frac{T'}{T_i}\right)\left(\frac{IE'}{IE_1}\right) + A_{10}\left(\frac{TH_i}{TH'}\right)\left(\frac{T'}{T_i}\right)\left(\frac{IE'}{IE_i}\right) + A_o \quad (27)$$

i = 1, 2, . . ., 11

where: T′ = 78°F; TH′ = 0.250 in., IE′ = 66.0 kJ (LW); IE′ = 27.5 kJ (SW)

Valid range:

190 ≤ TEIL (IE) ≤ 400 kJ; 25 ≤ EIS (IE) ≤ 200 kJ; 78 ≤ T_o(T) ≤ 550°F; 0.25 ≤ TH ≤ 1.125 in.

Measurements obtained from specimen sizes of:

5 ≤ ℓ ≤ 10 in. and 3 ≤ ω ≤ 5 in.

Table 14—Summary of Calculated Coefficients Used in Arriving at Equations (28) through (31) Shown in Appendix I

	Stationary Weld		Linear Weld	
	A	|B|	A′	|B|
A_1	4.558	1.615	1.405	−1.074
A_2	−38.552	−14.194	−11.057	−0.559
A_3	−273.263	−96.289	−16.473	−26.190
A_4	458.231	157.607	20.161	1.805
A_5	41.335	12.090	−803.402	−198.079
A_6	156.091	53.517	442.900	16.005
A_7	1.287	0.6561	3.774	10.027
A_8	17.397	6.9859	−6.207	29.794
A_9	−256.907	−87.028	72.779	122.811
A_{10}	−6.089	0.828	−31.697	−40.446
A_0	−64.243	−23.686	−2.569	0.432

of weld energy input, initial plate temperature, and section thickness are also included. After experimentally obtaining eleven values, through eleven experiments, of A, A′ and |B| and substituting them in the series relationship (Table 13), the computer was programmed to determine the various coefficients A_1, A_2, etc. The equations are written in normalized form so that the coefficients A_1 through A_o become dimensionless values.

Table 14 summarizes the resulting coefficients for the series expressions. Some of the coefficients, such as the last coefficient, $A_o = 0.342$, for |B| in the case of linear welds in Table 14, are small (less than 1). However, from equation (27) it is clear that the contribution of the last coefficient, A_o, would be about 33°F (0.5°C) (A_oT'), which is significant for the |B| value.

From the results shown in Table 14, a series of equations were developed to arrive at an estimate of the coefficients used in calculating the cooling rate for stationary and linear repair welds, respectively, in steel castings. These equations are summarized in Appendix I and will assist the welding engineer in predicting the maximum hardness in the HAZ to within a few Rc points. This system will permit the selection of welding conditions such that the maximum hardness encountered in the HAZ will be below the critical level required to prevent HIC.

Two examples of the complete calculation of the cooling rate employing the above equations and the maximum HAZ hardness of typical repair welds are included in the Appendix II.

Conclusions

The following conclusions pertain to the system for predicting maximum hardness in the weld heat-affected zone of cast steels:

1. A technique was developed to measure the temperature in the weld heat-affected zone at the fusion boundary.

2. Equations were derived by curve fitting the measured thermal cycles in the critical transformation temperature range from 700 to 1000°F (371 to 538°C) to enable the welding engineer to calculate the maximum cooling rate in the weld heat-affected zone.

3. With the aid of the system developed in this investigation, the maximum hardness in the HAZ can be predicted to within a few Rc points. However, the accuracy of this prediction is dependent on the homogeneity of the structure before repair welding is performed.

4. From calculations based upon the chemical composition and grain size, one can select the welding conditions (variables) that will ensure a safe level of maximum hardness in the HAZ.

Acknowledgments

The authors wish to thank Mr. Dan Stone and the Association of American Railroads (AAR) for their financial support of this project.

References

1. Jominy, W. E., and Boegehold, A. L. 1938 (June). A hardenability test for carburizing steels. *Trans. ASM.*

2. Field, J. 1943 (March). Calculations of end-quench hardenability from chemical composition. *Metal Progress.*

3. Hess, W. F., Merrill, L. L., Nippes, E. F., and Bunk, A. P. 1943. The measurement of cooling rates associated with arc welding and their application to the selection of optimum welding conditions. *Welding Journal* 22(9):377-s to 422-s.

4. Hess, W. F., Nippes, E. F., Merrill, L. L., and Bunk, A. P. 1944. Determination of cooling rates of butt and fillet welds as a result of arc welding with various types of electrodes on plain carbon steel. *Welding Journal* 23(8):376-s to 391-s.

5. Nippes, E. F., Merrill, L. L., and Savage, W. F. 1949. Cooling rates in arc welds in ½ inch plate. *Welding Journal* 28(11):SS6-s to 564-s.

6. Nippes, E. F., and Nelson, E. C. 1958. Prediction of weld heat-affected zone microstructures from continuous-cooling transformation data. *Welding Journal* 37(7):289-s to 294-s.

7. Pavelic, Vjekoslav. 1968 (May). *Temperature histories in a thin steel plate with tungsten inert gas process.* Ph.D. Thesis, Mechanical Engineering Department, The University of Wisconsin.

8. Alberry, P. J., and Jones, W. K. C. A computer model for the prediction of heat-affected zone microstructure in multipass weldments. The Metallurgical Society of AIME, TMS paper selection F79-12.

9. Rosenthal, D. Mathematical theory of heat distribution during welding and cutting. *Welding Journal* 20(5):220-s to 234-s.

10. Savage, W. F. 1980 (August). Private communication, Rensselaer Polytechnic Institute, Troy, New York.

Appendix

I. Summarized Coefficient Estimating Equations

$$A/_{T'} = 4.558\,(TH/_{TH'})^2 - 28.552\,(TH/_{TH'}) - 273.263\,(T'/_T)^2 + 458.231\,(T'/_T) + 41.335\,(1E'/_{1E})^2 + 156.091\,(1E'/_{1E}) + 1.287\,(TH/_{TH'})\,(T'/T) + 17.397\left(\frac{TH}{TH'}\right)\left(\frac{1E'}{1E}\right) - 256.907\left(\frac{T'}{T}\right)\left(\frac{1E'}{1E}\right) - 6.089\left(\frac{TH}{TH'}\right)\left(\frac{T'}{T}\right)\left(\frac{1E'}{1E}\right) - 64.243. \quad (28)$$

$$|B|/_{T'} = 1.614\left(\frac{TH}{TH'}\right)^2 - 14.194\left(\frac{TH}{TH'}\right) - 96.289\,(T'/_T)^2 + 157.607(T'/_T) + 12.080\left(\frac{1E'}{1E}\right)^2 + 53.517\,(1E'/_{1E}) + 0.6561\left(\frac{TH}{TH'}\right)\left(\frac{T'}{T}\right) + 6.9859\left(\frac{TH}{TH'}\right)\left(\frac{1E'}{1E}\right) -$$

$$87.028\,(T'/_T)\,(1E'/_{1E}) + 0.828\left(\frac{TH}{TH'}\right)\left(\frac{T'}{T}\right)\left(\frac{1E'}{1E}\right) - 23.686. \quad (29)$$

$$A'/_T = 1.405(TH/_{TH'})^2 - 11.057\left(\frac{TH}{TH'}\right) - 16.473(T'/_T)^2 + 20.161(T'/_T) - 803.402(1E'/_{1E})^2 + 442.900(1E'/_{1E}) + 3.774\left(\frac{TH}{TH'}\right)\left(\frac{T'}{T}\right) - 6.207\left(\frac{TH}{TH'}\right)\left(\frac{1E'}{1E}\right) + 72.779\left(\frac{T'}{T}\right)\left(\frac{1E'}{1E}\right) - 31.697\left(\frac{TH}{TH'}\right)\left(\frac{T'}{T}\right)\left(\frac{1E'}{1E}\right) - 2.569. \quad (30)$$

$$|B|/_{T'} = -1.074\left(\frac{TH}{TH'}\right)^2 - 0.559\left(\frac{TH}{TH'}\right) - 26.190(T'/_T)^2 + 1.805(T'/_T) - 198.079(1E'/_{1E})^2 + 16.005(1E'/_{1E}) + 10.027\left(\frac{TH}{TH'}\right)(T'/_T) + 29.794\left(\frac{TH}{TH'}\right)\left(\frac{1E'}{1E}\right) + 122.811\left(\frac{T'}{T}\right)\left(\frac{1E'}{1E}\right) - 40.446\left(\frac{TH}{TH'}\right)\left(\frac{T'}{T}\right)\left(\frac{1E'}{1E}\right) + 0.432. \quad (31)$$

II. Calculation Examples

1. *An example of predicting maximum hardness in the HAZ using a linear repair weld with the following conditions:* arc current – 220 A; arc voltage – 25 V; travel speed – 5 ipm; weld length – 3.5 in.; weld energy input, TEIL (IE) – 231 kJ; initial plate temperature, T_o (T) – 542 °F; section thickness, (TH) – 1.125 in.

To calculate A′ and |B|, substitute TH, T and IE values from above into equations (30) and (31), respectively, as shown below:

$$A'/_{T'} = 1.405\left(\frac{1.125}{0.25}\right)^2 - 11.057\left(\frac{1.125}{0.25}\right) - 16.473\,(78/_{542})^2 + 20.161\,(78/_{542}) - 803.402\,(66/_{231})^2 + 442.90\,(66/_{231}) + 3.773\left(\frac{1.125}{0.25}\right)(78/_{542}) - 6.207\left(\frac{1.125}{0.25}\right)\left(\frac{66}{231}\right) + 72.779\left(\frac{78}{542}\right)\left(\frac{66}{231}\right) - 31.697\left(\frac{1.125}{0.25}\right)\left(\frac{78}{542}\right)\left(\frac{66}{231}\right) - 2.569.$$

$$A'/_{T'} = 31.221;\ A' = 31.221\,(78) = 2435\ °F$$

$$|B|/_{T'} = -1.074\,(4.5)^2 - 0.559\,(4.5) - 26.190\,(0.144)^2 + 1.805\,(0.144) - 198.079\,(0.286)^2 + 16.005\,(0.286) + 10.027\,(4.5)\,(0.144) + 29.794\,(4.5)\,(0.286) + 122.811\,(0.144)\,(0.286) - 40.446\,(4.5)\,(0.144)\,(0.286) + 0.432$$

$$|B|/_{T'} = 6.664\,|B| = 6.664\,(78) = 520°F$$

Now substitute A′ and B in equation (2), *i.e.*, $T_i = A' + B\ \ln t$ and solve for t at $T_1 = 900°F$:

$$\ln t = \frac{900\text{-}2435}{-520}$$

$= 2.95$, $t = 19.14$ s, and

$$\frac{dT}{dt}\Big|_{900°F} = \frac{520}{19.14} = 27°F/s$$

(calculated cooling rate).

The measured values of A′ and |B| are 2512 and 525°F, respectively. Therefore, substituting these values in equation (2), the time t = 21.55 s. Therefore, the measured cooling rate

$$\frac{dT}{dt}\Big|_{900°F} = \frac{525}{21.55} = 24°F/s.$$

Now by combining equations (24) and (26) using JD (in 16th inches), the following equation can be written:

$$\frac{IH}{DH} = c + d\left\{\exp\left[\frac{5.50 - \ln(CR)}{1.32}\right]\right\}@900°F \quad (32)$$

IH, c and d are dependent on the heat chosen (*e.g.*, heat 27) IH = 51 Rc; and:

$D_I = 3.51$ in., c = 0.850 and d = 0.053 (see Table 12)

Substitute c and d in equation (32), *i.e.*,

$$\frac{IH}{DH} = 0.850 + 0.053\left\{\exp\left[\frac{5.50 - \ln(CR)}{1.32}\right]\right\}.$$

Using the above equation, the DH for measured cooling rate (24°F/s @ 900°F) will be 44 Rc and for calculated cooling rate (27°F/s @ 900°F) will be 45 Rc points.

2. *An example of predicting maximum hardness in the HAZ using a stationary repair weld with the following conditions:* arc current – 220 A; arc voltage – 25 V; arc time – 10 s; weld energy input, EIS (IE) – 55 kJ; initial plate temperature, T_o (T) – 390°F; section thickness, (TH) – 1.0 in.

To calculate A and |B|, substitute TH, T and 1E values from above into equations (28) and (29), respectively. Then A (calculated) = 2439 and A (measured) = 2384°F; |B| (calculated) = 656 and |B| (measured) = 682°F.

Using equations (1) and (3), the following measured and calculated cooling rates will be obtained:

$$\frac{dT}{dt}\Big|_{900°F} = 43°F/s \text{ (measured)}$$

$$\frac{dT}{dt}\Big|_{900°F} = 34°F/s \text{ (calculated)}$$

Using again heat 27, the measured DH and calculated DH (from equation (32)) will be 49 and 47 Rc, respectively.

AWS "Peer Review" Panel

The individuals whose names are listed below are participating in the "Peer Review" Program of the American Welding Society as it pertains to the Research Supplement of the *Welding Journal*. Participation consists of evaluating the technical content of papers submitted for publication in the Research Supplement and, to this end, rendering judgments concerning:

- Originality of the contribution.
- Technical value to the welding community.
- Prior publication of the material being reviewed.
- Proper credit to others working in the same technical area.
- Justification of the conclusions judging by the results.
- Degree of acceptability for publication.

It is considered that program participants are rendering an invaluable service to the welding community and to the authors of papers undergoing review. Others wishing to serve as reviewers are asked to contact the Technical Editor of the *Welding Journal*, P.O. Box 351040, Miami, FL 33135.

Current Reviewers

D. K. Aidun
G. A. Andreano
W. R. Apblett Jr.
D. G. Atteridge
W. G. Bader
W. A. Baeslack, III
J. C. Baker
D. J. Ball
C. M. Banas
R. E. Beal
F. Beaver
L. S. Beedle
C. R. Behringer
R. Beldyk
W. P. Benter, Jr.
J. T. Biskup
W. Borges
K. L. Brown
A. J. Bryhan
J. M. Cameron
D. A. Canonico
R. S. Chandel
D. U. Chang
R. A. Chihoski
M. Cieslak
N. S. Cole
C. E. Cross
S. A. David
R. DeNale
P. B. Dickerson
D. W. Dickinson
R. D. Dixon
R. B. Dooley
R. J. Dybas
T. W. Eagar
B. J. Eberhard
D. P. Edmonds
G. Edwards
J. W. Elmer
J. W. Fisher
E. A. Flynn
W. R. Frick
E. Friedman
L. M. Friedman
E. B. Gempler
J. M. Gerken
F. E. Gibbs
S. S. Glickstein
G. M. Goodwin
F. J. Grist
J. R. Hannahs
D. W. Harvey
D. C. Helton
R. T. Hemzacek
D. E. Hetzel
G. K. Hicken
T. Hikado
J. F. Hinrichs
D. G. Howden
E. I. Husa
J. E. Indacochea
C. E. Jackson
J. J. Jellison
J. E. Jones
P. A. Kammer
W. A. Kawahara
J. F. Key
R. A. Kelsey
J. F. King
W. H. King
G. A. Knorovsky
P. J. Konkol
L. J. Korb
D. J. Kotecki
S. Kou
J. S. Kozelski
F. V. Lawrence, Jr.
G. L. Leone
G. G. Lessmann
D. Link
J. C. Lippold
R. E. Long
C. R. Loper, Jr.
C. D. Lundin
K. A. Lyttle
A. F. Manz
R. P. Martukanitz
K. Masubuchi
D. K. Matlock
S. J. Matthews
R. B. McCauley
J. T. McGrath
H. I. McHenry
E. A. Metzbower
G. E. Metzger
J. A. Miller
J. W. Mitchell
A. J. Moorhead
W. H. Munse
T. M. Mustaleski
T. V. Natale
C. D. Nicky
E. F. Nippes
T. H. North
D. L. Olson
G. W. Oyler
V. J. Papazoglou
B. M. Patchett
D. W. Patterson
R. A. Patterson
A. W. Pense
D. D. Peter
E. Pfender
L. E. Pope
M. Prager
D. D. Rager
K. B. Rao
D. T. Read
W. S. Ricci
R. W. Richardson
G. D. Ries
A. M. Ritter
I. B. Robinson
M. N. Ruoff
E. P. Sadowski
W. W. Sanders, Jr.
L. W. Sandor
S. J. Santangelo
W. F. Savage
J. M. Sawhill, Jr.
M. M. Schwartz
E. G. Shifrin
L. E. Shoemaker
T. A. Siewert
G. M. Slaughter
J. P. Snyder, II
R. E. Somers
D. E. Spindler
J. Spingarn
G. R. Stoeckinger
R. D. Stout
M. A. Streicher
R. D. Sutton
J. R. Terrill
R. D. Thomas, Jr.
C. L. Tsai
A. J. Turner
G. D. Uttrachi
J. J. Vagi
T. L. VanderWert
R. Vasudevan
S. Venkataraman
R. C. Voigt
F. A. Wassell
T. A. Whipple
W. L. Wilcox
W. L. Winterbottom
C. E. Witherell
J. R. Woodward
K. C. Wu
H. Y. Yoon
C. A. Zanis